IEEE Access
Multidisciplinary ⋮ Rapid Review ⋮ Open Access Journal

Received November 7, 2019, accepted November 26, 2019, date of publication December 5, 2019, date of current version December 23, 2019.

Digital Object Identifier 10.1109/ACCESS.2019.2957949

Investigating Validity of Wide-Sense Stationary Assumption in Millimeter Wave Radio Channels

NAVEED IQBAL[1], (Student Member, IEEE), JIAN LUO[1], CHRISTIAN SCHNEIDER[2], DIEGO ANDRES DUPLEICH[2], ROBERT MÜLLER[2], STEPHAN HÄFNER[1], AND REINER S. THOMÄ[2], (Fellow, IEEE)

[1]Huawei German Research Center, 80992 München, Germany
[2]Institute of Information Technology, Technische Universität Ilmenau, D-98684 Ilmenau, Germany

Corresponding author: Naveed Iqbal (naveed.iqbal.q@gmail.com)

ABSTRACT In this paper, impact of antenna directivity and bandwidth on the small scale fading statistics have been analyzed for millimeter-wave (mmWave) radio channels. For this purpose, small-scale fading measurements at the mmWave frequency band (58–62 GHz) are carried out using transmit and receive antennas with different antenna directivities (emulated beamforming gains). Measurements emulate a non line-of-sight scenario when the communication between transmit and receive antennas is possible only through a single multipath cluster. In order to compare results, measurements in a line-of-sight scenario with omni-directional antennas are also carried out for reference purpose. Considering two main mmWave system features i.e., high antenna directivity and higher system bandwidth, we report the following results: 1) Randomness/fading in the received signal magnitude vanishes with an increase in bandwidth. 2) The channel impulse response $h(t, \tau)$ does not remain a wide-sense stationary (WSS) random process in the *slow–time* domain i.e., along t, where, the *fast–time* domain refers to the dimension along τ. 3) Measured channels are WSS in the frequency domain and the coherence bandwidth increases when propagation channels are illuminated with high gain antennas.

INDEX TERMS Small-scale fading, channel measurements, channel models, multipath clusters, beamforming, ultra-wide band (UWB) channels, millimeter wave (mmWave) communications, MIMO, 5G.

I. INTRODUCTION

System assumptions such as bandwidth and beamforming gain from antenna arrays play a vital role in defining the channel modeling methodology. For example, 3GPP-LTE systems [1] apply spatial pre– and post– processing to narrowband channels (e.g., one subcarrier obtained after orthogonal frequency division multiplexing (OFDM)). Since, the antenna directivity in 3GPP-LTE systems is quite low, standardized channel models for these systems such as 3GPP-SCM [2], WINNER [3] and COST-2100 [4], are based on the rich multipath scattering assumption in both line-of-sight (LOS) and non-LOS (NLOS) scenarios. Consequently, complex Gaussian random variable (RV) assumption holds for each subcarrier and the resulting channels can be modeled as Rice and Rayleigh fading channels. These subcarriers are correlated up to the coherence bandwidth and the propagation channels are wide-sense stationary (WSS) in the frequency-domain. In the delay-domain, this corresponds to uncorrelated scattering of delay resolvable multi-paths components (MPCs) which are often denoted as multipath clusters.[1] Additionally in the models [2]–[4], due to the complex Gaussian RV assumption per subcarrier, the number of stochastic degrees-of-freedom (DOF) in the frequency-domain increases linearly with bandwidth.

For LOS and NLOS scenarios in [2]–[4], an independent-and-identically-distributed (i.i.d.) complex Gaussian channel impulse response (CIR) results in Rice and Rayleigh

The associate editor coordinating the review of this manuscript and approving it for publication was Vittorio Degli-Esposti.

[1]In this paper, a cluster is defined as a group of MPCs in the propagation channel which depart and arrive in the same direction and nearly have same arrival time (delay time) at the receiver.

multipath channels, respectively.[2] Consequently, similar to Rayleigh–Rice models, both LOS and NLOS channels in [2]–[4] are also WSS in slow-time within a local area. In such a case, the receive signal magnitude—square root of the total power[3]—also becomes a WSS random process within a local area. From a system design perspective, large variations in the received signal magnitude lead to an increased level crossing rate and higher outage probabilities [5]. These quantities have implications on the beam handover protocols and frame structure design, which are required to maintain a communication link.

Similar to the models [2]–[4], multipath modeling methodology in the state-of-the-art (SOTA) mmWave channel models [6]–[13] is also based on the WSS assumption; both in the frequency-domain and in the slow-time domain. In general, it is quite plausible that a multipath channel is WSS in the frequency domain but the CIR violates WSS assumption over slow-time domain due to wider bandwidth. In contrast to the 3GPP-LTE systems, mmWave systems are supposed to operate with highly directive antennas to mitigate higher path losses. A highly directive beamformer may do the spatial filtering of a multipath channel, e.g., it may illuminate only a single, strong and a potentially sparse multipath cluster. In such a case, the central limit theorem cannot be applied. Consequently, modeling the propagation channel in such a way that each subcarrier is a complex Gaussian random variable, becomes questionable. Apart from high beamforming gain, mmWave systems are supposed to be wideband due to the large absolute bandwidths available at these frequencies. When the overall channel bandwidth becomes wider, the application of complex Gaussian CIR assumption over time also becomes questionable.

On noting differences between theoretical expectations and SOTA channel models for mmWave systems, validity of narrowband WSS assumption in mmWave radio channels becomes a question of fundamental interest. This is the primary scope of this contribution. With the best of our knowledge, no such work exists in the mmWave channel modeling literature. Note that, we used the same measurement data as in our earlier contributions [14]–[17], but the scope of this work is different and reported results are novel.

The paper is organized as follows: Details about the measurement campaign and channel data processing are described in Section II and Section III, respectively. One of the objectives of Section IV is to investigate complex Gaussian CIR assumption in slow-time, which results in constant mean (roughly) and variances of the receive signal magnitude in a local area. Moreover, validity of the WSS assumption in the frequency domain is also investigated in Section IV. Finally, conclusions are drawn in Section V.

[2]Notice that, earlier discussions focused on the complex Gaussian RV assumption in the frequency domain i.e., per subcarrier. In contrast, here we discuss about complex Gaussian CIR assumption i.e., along the delay domain.

[3]By total power, we mean absolute square integrated over all subcarriers—assuming that the transmitter (Tx) allocates equal power to each subcarrier.

II. MEASUREMENT SCENARIO AND THE EXPERIMENTAL SETUP

A. CHANNEL SOUNDER

Channel measurements are conducted through ultra-wide band (UWB) transmit (Tx) and receive (Rx) channel sounding units which have been introduced earlier in [18]. After calibration, channel sounder offers an instantaneous 3-dB absolute bandwidth of 4 GHz with a dynamic range up to 70 dB. The sounding signal is a chip sequence of length 4095 with a chiprate of 6.75 GHz. Both Tx and Rx sounding units are synchronized to the same clock via cables resulting in a highly stable relative delay between the sounder units.

B. EXPERIMENTAL SETUP

Experiments are conducted in a typical laboratory room with a plenty of equipment placed in the vicinity of both transmitter (Tx) and Rx, as shown in Fig. 1. Position of Tx is kept fixed, however, Rx moves towards the wall on a linear positioning device denoted as *rail*, as shown in Fig. 2. Both LOS and NLOS[4] measurements are conducted and with Tx-Rx antenna setups shown in Table 1, which are detailed as follows:

- In the LOS case, omni-directional antennas are used at both Tx and Rx. Small-scale fading measurements are conducted using the experimental setup, rail position and Rx movement direction as shown in Fig. 2.
- In the NLOS case, only a particular spot on the wall is illuminated with a 15° half power beam width (HPBW) Tx antenna. Incident point in the wall is 2.6 meter away from the Tx, which is far beyond the Fraunhofer distance (31mm) to ensure plane wave propagation. As a result, Tx antenna footprint on the surface of the wall is approximately 0.4 m^2. At the Rx side, both directional (always pointed towards the incident point) and omni-directional antennas are used. Directional illumination with 15° HPBW Rx antenna, when placed at 4.8m away from the surface of wall, leaves an antenna footprint of 1.25 m^2 which reduces up to 0.4 m^2 when Rx reaches at the terminal point of its movement. Similarly, when a 30° HPBW Rx is employed, the antenna footprint on the surface of wall reduces from 5.2 m^2 up to 0.7 m^2 as Rx moves closer to the wall. Note that, when low gain Rx antennas are employed, a cross-talk between Tx-Rx antennas may result in a possible violation of our NLOS definition. However, we emphasize that, the energy contributions of these cross-talk effects is negligible. Consequently, the measurements with low gain Rx antennas approximately fulfill our NLOS definition. During measurements, Tx and Rx antenna pointing angles are adjusted such that the intersection area of their footprints on the surface of the wall imitate a geometry-based multipath cluster [19].

[4]Although, measurements consider perfect optical visibility between Tx&Rx, the setup is still referred to as NLOS, because directional antennas are not pointed towards each other.

FIGURE 1. Picture of the environment and fading measurement setup.

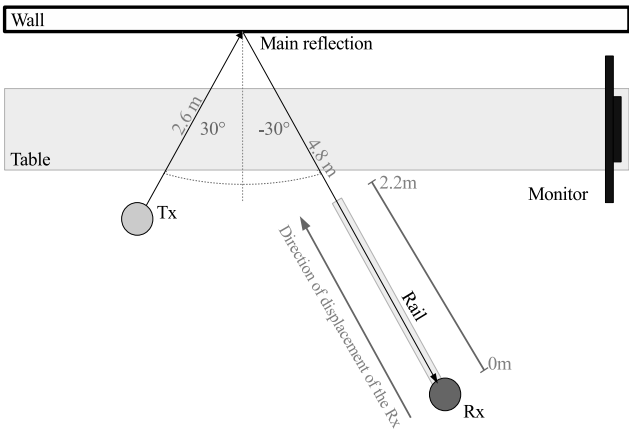

FIGURE 2. Top-view schematic of the radio channel fading measurement set-up.

For both LOS and NLOS measurements, same experimental setup shown in Fig. 2 is used, while maintaining the rail position and direction of motion of Rx i.e., towards the wall. Note that, high resolution antennas (greater than 15° HPBW) have been intentionally avoided during the measurements, as this may lead a situation when only a single MPC is illuminated instead of a cluster. Thus resulting in a measured channel with a no random process to model. In order to track changes in the time-varying propagation channel, at least two snapshots per wavelength should be measured [20]. Therefore, Rx movement step size is fixed to $\frac{\lambda_c}{2} = 2.5$mm, where, λ_c corresponds to a wavelength at 60 GHz center frequency. In this way, Rx is moved on the rail towards the wall, covering a 2.2m long track in a local area. These linear Rx movements result in measuring a total of 881 time snapshots along the track. Three synchronized PCs are used to control linear Rx movements along the rail, switches for the polarization and record the data sent by the UWB sounding units. Rest of the measurement channel parameter values are summarized in Table 1.

III. POST-PROCESSING OF THE MEASURED CHANNEL DATA

At first, the measured CIR $h(t,\tau)$ is processed by estimating a noise floor N_f in dB, using a post-procedure described in [21]. After that all the time domain samples below $N_f + 10$ dB are zeroed out. Finally, a 25 dB dynamic range is applied to the CIR. Let $H(t,f)$ corresponds to a channel

TABLE 1. Channel sounding and measurement parameters.

Parameters	Values
Center frequency (f_c)	60 GHz
Measured bandwidth	3 dB bandwidth of 4 GHz
Tx/Rx height	1.52 m
Rx antenna HPBW	15° (21 dBi) | 30° (14 dBi) | Omni (0 dBi)
Tx antenna HPBW	15° (21 dBi) | Omni (0 dBi)
Measured radio channel setups and their visibility	Tx 15° HPBW, Rx 15° HPBW→NLOS Tx 15° HPBW, Rx 30° HPBW→NLOS Tx 15° HPBW, Rx Omni→NLOS Tx Omni, Rx Omni → LOS
Tx-Rx antenna polarization setup	Vertical-Vertical
Rx movement step size	2.5 mm

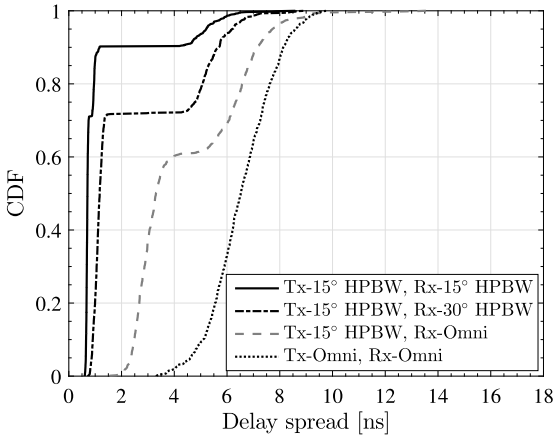

FIGURE 3. Root mean square (rms) delay spread statistics over the whole measurement track.

transfer function (CTF) obtained after discrete fourier transform (DFT) of the complex CIR $h(t,\tau)$. We assume that $H(t,f)$ is approximately frequency flat, which is quite plausible assumption for both LOS and NLOS measurements due to the small delay spread (DS) values (large coherence bandwidth) shown in Fig. 3. In the LOS case, most of the Rx signal energy is carried by the LOS path, resulting in small DS values, as shown in Fig. 3. In the NLOS case, small DS values come from the fact that Tx illuminates only a particular spot on a reflection surface as shown in Fig. 2 with a narrow 15° HPBW antenna. Let n_f (= 3095) be the total number of frequency samples with an absolute bandwidth 1.3 MHz per

sample after calibration. Now the CTF at a particular time instant t on the rail can be expressed as

$$H(t,f) = \sum_{n=1}^{n_f} A(t,n)\, e^{j\theta(t,f)} \delta(f - n\Delta f) \tag{1}$$

where, A and θ correspond to magnitude and phase responses of the channel at the n^{th} frequency bin. For bandwidth reduction (if required), frequency domain samples are extracted while maintaining the center frequency f_c and length of the full-band frequency domain channel such that

$$H_W(t,f) = \begin{cases} H(t,f), & f_l \le f \le f_h \\ 0 & \text{otherwise.} \end{cases} \tag{2}$$

Now the channel absolute bandwidth W is defined as $W = f_h - f_l$, where, f_h and f_l are the highest and lowest frequencies of the band, respectively. Time domain CIR vector $h_W(t,\tau)$ is obtained by inverse Fourier transform of $H_W(t,f)$. From the Parseval relation, the total receive signal magnitude is defined as $E_{\text{Rx}}(t) = \sqrt{\int_0^\infty |h_W(t,\tau)|^2\, d\tau} = \sqrt{\int_{-\infty}^{\infty} |H_W(t,f)|^2\, df}$. In this paper, measured CTF $H_W(t,f)$ is normalized such that the ensemble average of Rx magnitude over all Rx positions is $\rho = \mathcal{E}(E_{\text{Rx}}(t)) = 1$. This normalization removes the global pathloss due to an initial Tx-Rx distance of each measurement. However, local pathloss or path gain effect due to the Rx movement afterwards on the rail is maintained.

IV. STATISTICAL CHARACTERIZATION OF MEASURED CHANNELS

Objective of statistical characterization, in this section, is to study the impact of high antenna directivity and system bandwidth on WSS of the Rx signal. A random process is said to be WSS if its mean, variance and auto-correlation function (ACF) are time– or shift– invariant.

A. WSS IN THE RX SIGNAL MAGNITUDE

By definition, a stationary random process always return towards its mean value and it does not show any specific increasing/decreasing trend. Consequently, the mean value of a stationary process remains constant over the whole observation interval. Intuitively, when small-scale fading dominates over the large-scale fading effects in a channel, then a deterministic increasing/decreasing trend (due to path-loss) in the Rx magnitude may vanish. Consequently, the Rx signal magnitude appears to be a stationary random process within a fading interval. On the other hand, in the absence of small-scale fading, the Rx signal magnitude is expected to be a non-stationary process due to the dominance of path-loss. A visual inspection of results in Fig. 4 demonstrates that, in contrast to the narrowband channels, Rx magnitude shows an increasing trend for high bandwidth channels when illuminated with high gain antennas.

In general, propagation channel parameters evolve with time and displacement when either of the Tx or Rx moves

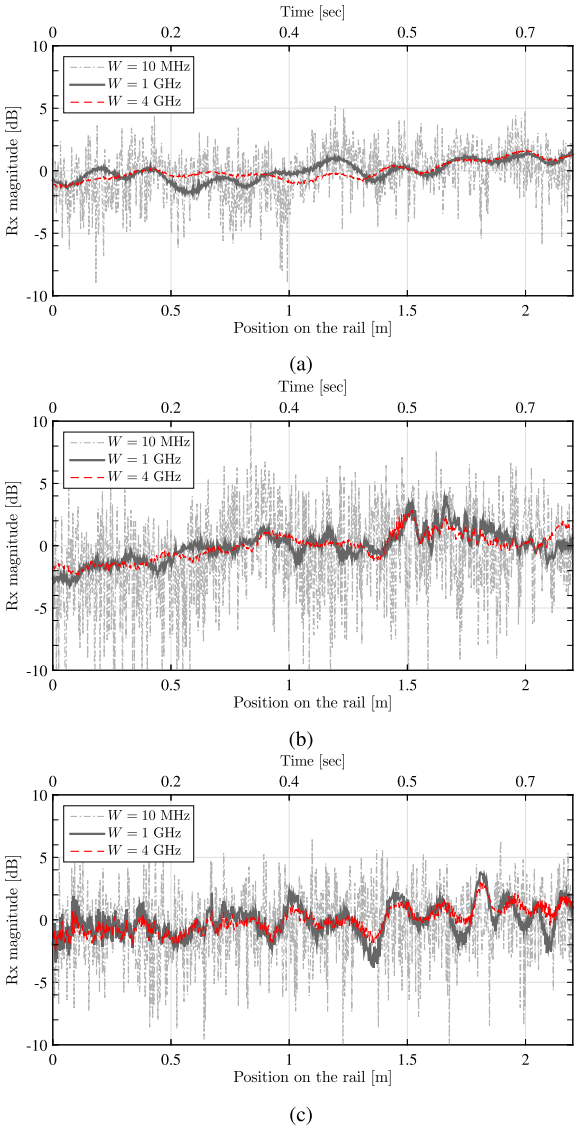

FIGURE 4. Rx signal magnitude (relative to the 0 dB mean value) analysis over the whole measurement track, VV polarization, speed of the Rx is equal to 10 kilometer per hour, (a) NLOS, Tx 15° HPBW, Rx 15° HPBW. (b) NLOS, Tx 15° HPBW, Rx-Omni. (c) LOS, Tx-Omni, Rx-Omni.

in a certain direction. Consequently, channel snapshots at adjacent Tx–Rx positions are supposed to be correlated. This results in a time series that can be described by an arbitrary difference (or differential) equation. In order to analyze WSS of this time series, roots of the characteristic equation (corresponding to the difference equation of time series) need to be analyzed. If there exists at least one *unit root*[5] then it implies that mean, variance and ACF are time-variant which result in a non-WSS time series. We use the Dickey-Fuller (DF) test [22] with a null hypothesis that the process contains at least one unit root. A rejection of null hypothesis implies that, Rx magnitude is a stationary random process over the whole measurement track and acceptance explains

[5]Solution set to the characteristic equation contains a root with an absolute value equal to 1.

TABLE 2. Results obtained from Dickey-Fuller test.

Visibility	Setup	Absolute bandwidth (GHz)								
		0.01	0.05	0.1	0.3	0.5	0.7	1	2	4
NLOS	Rx 15° HPBW, Tx 15° HPBW	-23.76 (R)	-12.05 (R)	-7.1 (R)	-3.2 (A)	-2.7 (A)	-2.4 (A)	-2.2 (A)	-2.1 (A)	-2.08 (A)
NLOS	Rx 30° HPBW, Tx 15° HPBW	-24.84 (R)	-10.83 (R)	-8.7 (R)	-3.1 (A)	-2.6 (A)	-2.3 (A)	-2.04 (A)	-1.7 (A)	-2.01 (A)
NLOS	Rx Omni, Tx 15° HPBW	-26.7 (R)	-21.4 (R)	-17 (R)	-17.7 (R)	-14.3 (R)	-8 (R)	-4.4 (R)	-3.3 (A)	-3.3 (A)
LOS	Rx Omni, Tx Omni	-28.6 (R)	-21 (R)	-24.5 (R)	-15.9 (R)	-12 (R)	-9.5 (R)	-8.5 (R)	-8.4 (R)	-7.6 (R)

that the time series is non-stationary. Accept (A) and reject (R) decisions are based on the critical value (CV) of -3.43 (1 % significance), where the values lower than the CV result in a rejection of null hypothesis and vice versa. As expected, test statistics in Table 2 show that, Rx signal magnitude does not remain a stationary random process for high bandwidth and high gain antenna systems.

B. VARIANCE OF THE RX MAGNITUDE

We now analyze the temporal variability of variance of the Rx signal magnitude as function of bandwidth and antenna directivity. In general, a small-scale fading area is defined such that channel statistics does not vary considerably and the Rx signal remains a stationary random process. An exact length of the stationary interval is hard to define [23], because radio channel statistics are strongly coupled with the properties of system under consideration, as shown in this paper. Length of the stationarity (i.e., $30\lambda_c$) interval, in this work, is largely based on the visual inspection which may not be very accurate for each measurement setup. A smaller length ($< 30\lambda_c$) may be more appropriate, but $30\lambda_c$ is chosen because authors wished to have enough measured channel snapshots as well, for better statistical accuracy. For this purpose, an overlapping sliding window of length $30\lambda_c$ is moved over the whole 2.2m long measurement track. This results in an extraction of 822 small-scale fading areas each of length $30\lambda_c$. For each of these intervals, irrespective of any W, mean value of $E_{\mathrm{Rx}}(t)$ is maintained as $\rho = 0$ dB due to the normalization. Thus allowing only the standard deviation (σ_0) of $E_{\mathrm{Rx}}(t)$ to change along different fading intervals and for different measurement setups. Intuitively, a high similarity of σ_0 values over the measurement track indicates that, σ_0 is time-invariant (a requirement of WSS) and vice versa. Two interesting observations are evident from results in Fig. 5,

- Fading of the Rx signal magnitude vanishes because the average spread ($\bar{\sigma}_0$) reduces with W up to a bandwidth $W_0 = 2.5$ GHz, known as stability bandwidth [24]. For bandwidth $W > W_0$, there are no significant changes in the radio channel from fading perspectives.
- For narrow-band channels, σ_0 values for different fading intervals are almost same, demonstrating that $E_{\mathrm{Rx}}(t)$ is nearly a stationary process over the whole measurement track. However, same is not true for wide-band channels as the spread of σ_0 increases for higher bandwidth channels demonstrating that Rx signal becomes a non-stationary random process.

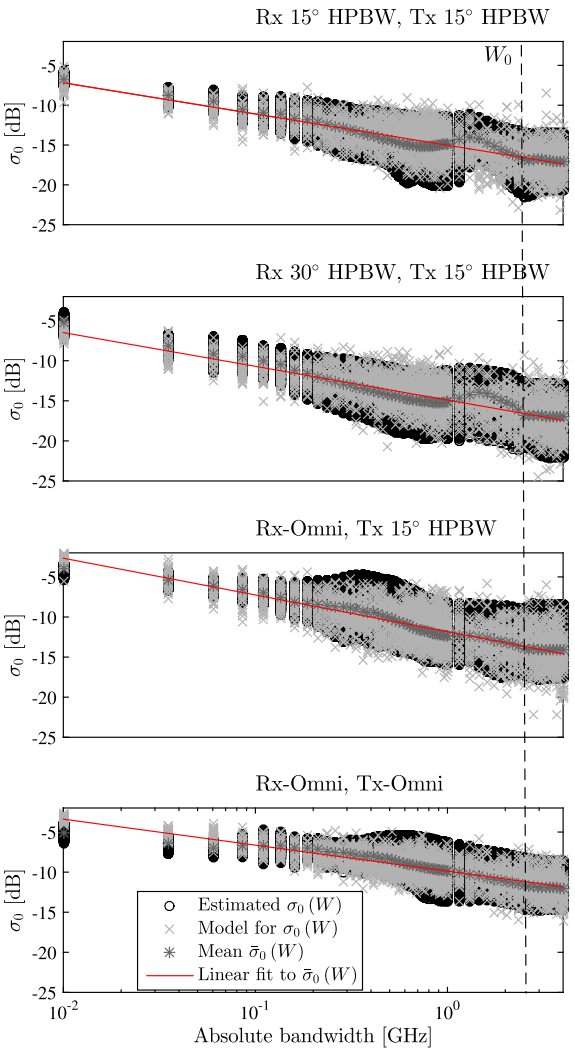

FIGURE 5. Measured and modeled values of $\sigma_0(W)$ while maintaining $\rho = 0$ dB mean value due to the channel normalization.

Intuitively, one cannot expect from a propagation environment to favor one stationary interval over the other. Therefore,

TABLE 3. Proposed models for the mean $\bar{\sigma}_0(W)$ and standard deviation $\mathcal{X}_{\sigma_0}(W)$ of σ_0 and their parameter values.

Visibility	Measurement setup	Model and parameter values $\bar{\sigma}_0(W) = \begin{cases} c_0 - m\log_{10} W, & \text{if } W \le W_0 \\ c_1 & \text{otherwise} \end{cases}$			Model and parameter values $\mathcal{X}_{\sigma_0}(W) = c_0 + m\log_{10} W$	
		Slope m (95% confidence bounds)	Intercept c_0 (95% confidence bounds)	c_1	Slope m (95% confidence bounds)	Intercept c_0 (95% confidence bounds)
NLOS	Rx 15° HPBW, Tx 15° HPBW	3.9 (4.2,3.7)	-15 (-15.1,-14.9)	-16.7	0.5 (0.36,0.6)	1.7 (1.66,1.8)
NLOS	Rx 30° HPBW, Tx 15° HPBW	4.2 (4.5, 3.8)	-14.9 (-15.1,-14.7)	-16.7	0.6 (0.54,0.7)	1.86 (1.82,1.9)
NLOS	Rx Omni, Tx 15° HPBW	4.6 (4.8, 4.4)	-11.8 (-11.9,-11.7)	-13.8	0.63 (0.4,0.8)	2 (1.9,2.1)
LOS	Rx Omni, Tx Omni	3.2 (3.5,3)	-9.9 (-10,-9.7)	-11.2	0.5 (0.4,0.6)	1.28 (1.2,1.33)

σ_0 is modeled as a normally distributed random process $\mathcal{N}\left(\bar{\sigma}_0(W), \mathcal{X}_{\sigma_0}(W)\right)$, where, $\mathcal{X}_{\sigma_0}(W)$ is the spread of σ_0 at a particular bandwidth W. Results in Fig. 5 show that, σ_0 obtained from 822 measured stationary intervals is an increasing function of W around $\bar{\sigma}_0(W)$ which demonstrates that Rx signal magnitude becomes non-WSS. This is indicated by the positive slopes m in the slope-intercept model of $\mathcal{X}_{\sigma_0}(W)$ in Table 3. One may note that, an increase in $\mathcal{X}_{\sigma_0}$ is not monotonic with W. However, an approximation of $\mathcal{X}_{\sigma_0}(W)$ with a slope-intercept form in Table 3 is done to maintain simplicity and intuitiveness. Fig. 5 shows that, the slope-constant model with parameter values in Table 3 provides a very good approximation of $\bar{\sigma}_0(W)$ and same is the case for slope-intercept model derived for variance of $\sigma_0(W)$.

C. WSS IN THE CHANNEL IMPULSE RESPONSE OVER THE SLOW-TIME

Now we intend to analyze if the channel temporal ACF $c_h(\Delta t, \tau) = E\left[h(t+\Delta t, \tau)\, h^*(t, \tau)\right]$ is shift- or time-invariant—a requirement for CIR to be WSS in the slow time. Let $\mu_{II}(\Delta t, \tau)$ and $\mu_{QQ}(\Delta t, \tau)$ are ACFs of inphase (I) and quadrature (Q) components and $\gamma_{IQ}(\Delta t, \tau)$ is their temporal cross-correlation, then real ($\Re$) and imaginary ($\Im$) parts of $c_h(\Delta t, \tau)$ are defined as

$$\Re\{c_h(\Delta t, \tau)\} = \mu_{II}(\Delta t, \tau) + \mu_{QQ}(\Delta t, \tau) \tag{3}$$

and

$$\Im\{c_h(\Delta t, \tau)\} = \gamma_{IQ}(\Delta t, \tau) - \gamma_{QI}(\Delta t, \tau)\cdot \tag{4}$$

where,

$$\mu_{II}(\Delta t, \tau) = E\left[h_I(t+\Delta t, \tau)\, h_I^*(t, \tau)\right] \tag{5}$$
$$\mu_{QQ}(\Delta t, \tau) = E\left[h_Q(t+\Delta t, \tau)\, h_Q^*(t, \tau)\right] \tag{6}$$
$$\gamma_{IQ}(\Delta t, \tau) = E\left[h_I(t+\Delta t, \tau)\, h_Q^*(t, \tau)\right] \tag{7}$$
$$\gamma_{QI}(\Delta t, \tau) = E\left[h_Q(t+\Delta t, \tau)\, h_I^*(t, \tau)\right]\cdot \tag{8}$$

A real valued $c_h(\Delta t, \tau)$ is possible when $\gamma_{IQ}(\Delta t, \tau) = \gamma_{QI}(\Delta t, \tau) = 0,\ \forall \Delta t \ge 0$, which leads to a fact that complex Rx signal is a circularly symmetric complex Gaussian random variable and the channel corresponds to a rich scattering environment [25]. Using the same measurement data, validity of the narrowband rich scattering assumption has been analyzed in our earlier work [17]. Results in [17] demonstrated that rich scattering assumption does not remain valid due to high gain antennas and higher bandwidth of mmWave systems. Consequently, Rayleigh–Rice fading channels for the cluster fading envelope are not realistic.

In general, for non-Gaussian signals, second-order statistics of a time domain signal are not fully described by $c_h(\Delta t, \tau)$ [25], [26]. Therefore, another function, denoted either as relation function $r_h(\Delta t, \tau) = E[h(t+\Delta t, \tau)\, h(t, \tau)]$ [25] or complementary ACF (CACF) [26] is used which measures a correlation between $h(\Delta t, \tau)$ and $h^*(\Delta t, \tau)$. From hereinafter, in the subsequent discussions, $r_h(\Delta t, \tau)$ is referred to as CACF. The real and imaginary parts of the CACF are defined as

$$\Re\{r_h(\Delta t, \tau)\} = \mu_{II}(\Delta t, \tau) - \mu_{QQ}(\Delta t, \tau) \tag{9}$$

and

$$\Im\{r_h(\Delta t, \tau)\} = \gamma_{IQ}(\Delta t, \tau) + \gamma_{QI}(\Delta t, \tau)\cdot \tag{10}$$

A CACF provides following insights into the channel properties:

- $r_h(\Delta t = 0, \tau) = 0$ implies that the channel $h(t, \tau)$ is a circularly symmetric random variable—a requirement for Rayleigh–Rice fading signals; analyzed in our earlier work [17].
- Vanishing of CACF $r_h(\Delta t, \tau) \approx 0,\ \forall \Delta t$ implies that $c_h(\Delta t, \tau)$ is time-invariant—a requirement for WSS signal [27], [28]. Therefore, following two conditions must be satisfied,

$$\mu_{II}(\Delta t, \tau) = \mu_{QQ}(\Delta t, \tau) \tag{11}$$

and

$$\gamma_{IQ}(\Delta t, \tau) = -\gamma_{QI}(\Delta t, \tau)\cdot \tag{12}$$

These conditions imply that, for a CIR to be WSS in slow time, the I and Q components must be balanced in the sense

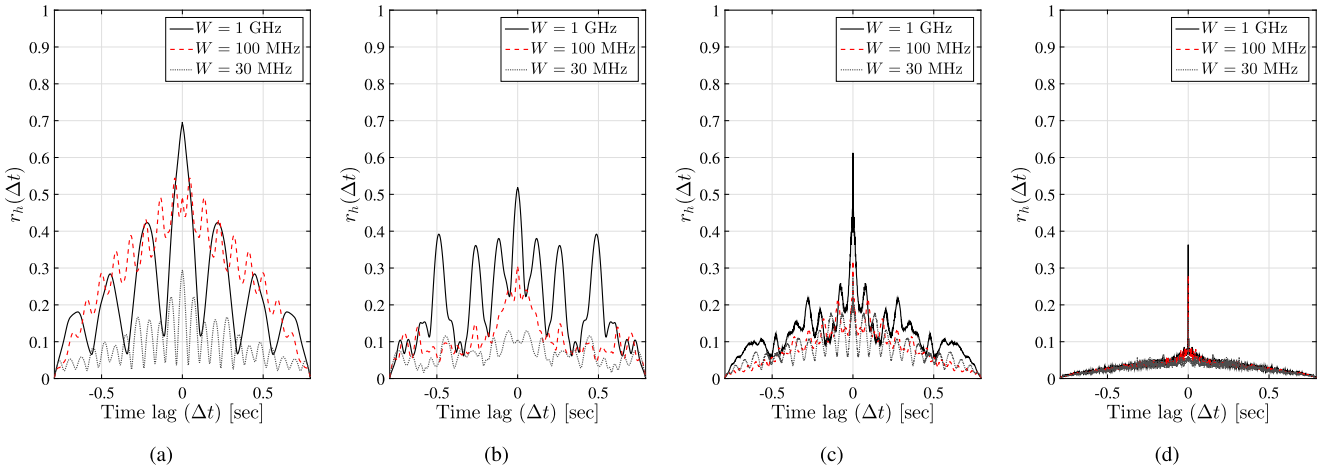

FIGURE 6. Analysis of CACF (averaged over multipath delays) for WSS testing. Speed of the Rx is equal to 10 kilometer per hour, (a) NLOS, Tx 15° HPBW, Rx 15° HPBW. (b) NLOS, Tx 15° HPBW, Rx 30° HPBW. (c) NLOS, Tx 15° HPBW, Rx-Omni directional. (d) LOS, Tx-Omni, Rx-Omni directional.

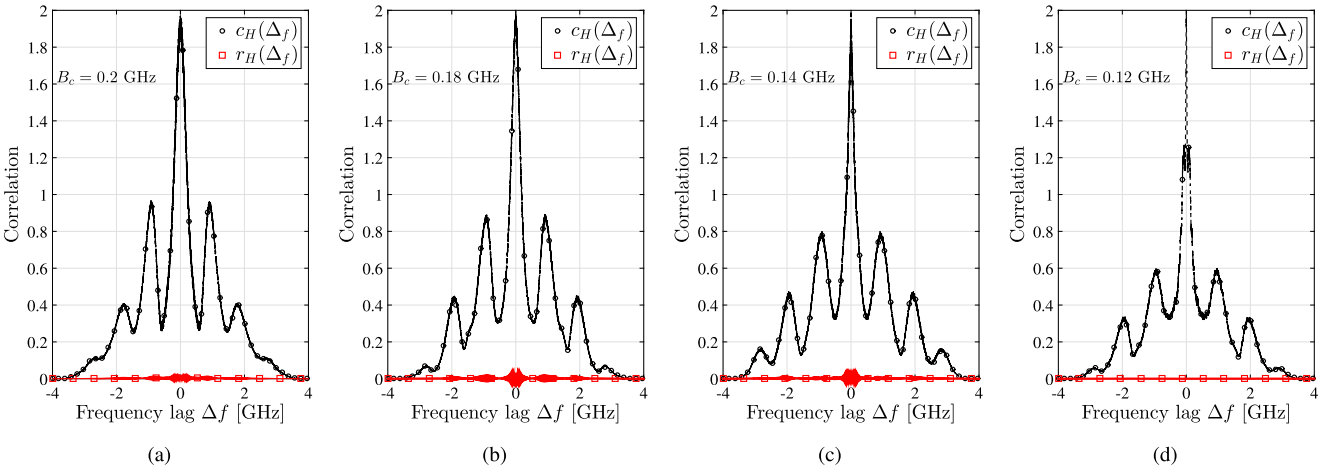

FIGURE 7. Correlation analysis of CTF (averaged over each time snapshot) for the testing of WSS in frequency domain. Speed of the Rx is equal to 10 kilometer per hour, (a) NLOS, Tx 15° HPBW, Rx 15° HPBW. (b) NLOS, Tx 15° HPBW, Rx 30° HPBW. (c) NLOS, Tx 15° HPBW, Rx-Omni directional. (d) LOS, Tx-Omni, Rx-Omni directional.

that their ACFs are the same and their cross-correlation function $\gamma_{IQ}(\Delta t, \tau)$ is an odd function. For each measurement setup, results in Fig. 6 show CACFs (averaged over path delays) for different bandwidth channels. It is interesting to note that, when high gain antennas are used, $r_h(\Delta t)$ does not vanish to zero even for narrowband channels (e.g. 30 MHz and 100 MHz). In contrast, an increasing trend in values of $r_h(\Delta t)$ is quite evident with an increase in bandwidth and antenna gain. However, when omni-directional antennas are used, the measured CIR demonstrates properties quite closer to a WSS signal. As expected, an increase in system bandwidth also have a profound impact on the complex CIR which becomes non-WSS in high bandwidth channels.

D. WSS IN FREQUENCY DOMAIN

For a time varying CTF $H_W(t, f)$, this section aims to analyze WSS in the frequency domain; uncorrelated scattering in the delay domain. This means that, at a particular time instant t, the channel frequency correlation function (FCF)

$$c_H(t, \Delta f) = E\left[H(t, f + \Delta f) H^*(t, f)\right] \tag{13}$$

depends only on the frequency lag $\Delta f = f_2 - f_1$. This means that, $c_H(t, \Delta f)$ does not depend upon the absolute frequency f. Similar like complex Gaussian CIR, $H(t, \Delta f)$ is a complex Gaussian random process in frequency (hence WSS), if the second-order statistics are fully described by $c_H(t, \Delta f)$ and complementary auto-correlation function

$$r_H(t, \Delta f) = E\left[H(t, f + \Delta f) H(t, f)\right] \tag{14}$$

is zero for all $\Delta f \geq 0$. All results in Figs. 7a to 7d show that, the time averaged $r_H(\Delta f) \approx 0$ for the whole frequency lag Δf. This implies that the function $c_H(t, \Delta f)$ in (13) is independent of absolute frequency and measured channels are WSS in the frequency domain.

Assuming that, the frequency domain samples in the CTF are decorrelated when $c_H(t, \Delta f)$ is less than 50% of the peak

correlation value, then the coherence bandwidth B_c evaluated from the measured channels is shown in Fig. 7. As expected from the delay spread statistics in Fig. 3, the coherence bandwidth is quite large i.e., $B_c = 0.2$ GHz in the case when highly directive 15° HPBW Tx-Rx antennas are employed. However, coherence bandwidth reduces when less directive antennas are used at Rx. In the LOS case, when omni-directional antennas at both Tx-Rx are used to illuminate the channel, coherence bandwidth is lowest, i.e., $B_c = 0.12$ GHz.

V. DISCUSSION AND CONCLUSION

High bandwidth and high beamforming gain are the features that distinguish mmWave systems from the conventional narrowband sub 6 GHz systems. For sub 6 GHz systems, success and simplicity of the corresponding geometry-based stochastic channel models [2]–[4] owes its origin to the narrowband assumptions in these models. In a sequence of contributions [14]–[17], [29]–[31], we have reported that fade depth of a Rx signal vanishes in spatially-filtered (due to high gains antennas) and delay-resolved (due to high system bandwidth) radio channels. Thus, resulting in radio channels with a considerably reduced small-scale fading. For these channels, discussions in [15] provide insights into how a sparse illumination of a propagation channel reduces Doppler spread. Therefore, in contrast to Doppler spread, concept of Doppler shift experienced by each MPC gains more importance in the multipath modeling. Additionally, randomness in the polarization coupling matrix vanishes with bandwidth [30], [32]. Therefore, cross-polarization power ratio (XPR) cannot be modeled as log-normal random process. Results in [31] show that, intra-cluster number of MPCs is small, and therefore Rayleigh-Rice channels are not realistic models for the cluster fading envelope. In contrast to [2]–[4] where each cluster has Rayleigh fading Rx envelope with zero-mean and unit variance, results in [31] show that Rx envelope of each multipath cluster from a different reflection surface differs considerably, demonstrating that mmWave frequencies are more sensitive to reflection surfaces.

In this contribution, we extended our studies presented in [14]–[17], [29]–[31] and focused on analyzing impact of antenna directivity and bandwidth on the validity of WSS assumption in the slow-time and in the frequency domain. It has been shown that:

1) Rx magnitude does not remain a stationary random process in the slow time and it shows a semi-deterministic trend in fading with Rx movement.
2) Variance of the Rx magnitude varies considerably for different fading intervals over the measurement track.
3) When directivity and/or bandwidth increases, the radio CIR in the slow time does not remain a WSS. This means that i.i.d. complex Gaussian CIR assumption as that of Rayleigh–Rice channels cannot be applied. In this way, we also negate some of our previous results in [14]–[16], where Rician multipath model is proposed.
4) Measured channels are WSS in the frequency domain and the coherence bandwidth increases with an increase in antenna directivity.

From the results and discussions above, we conclude that the channel modeling methodology in 3GPP-TR 38901 [6] (inherited from [2]–[4]) and other SOTA channel models does not meet on theoretical expectations on WSS imposed by high antenna directivity and bandwidth of mmWave systems. Therefore, for accurate performance prediction of mmWave systems, channel modeling methodology in SOTA channel models need to be revised. These revisions and concept validations must be supported by extensive measurements and data evaluations.

REFERENCES

[1] *Evolved Universal Terrestrial Radio Access (E-UTRA) Physical Channels and Modulation*, document 3GPP 36.211 V10.2.0, Jan. 2011.
[2] *Spatial Channel Model for Multiple Input Multiple Output (MIMO) Simulations*, document 3GPP 25.996, Version 12.0.0, Release 12, Sep. 2014.
[3] P. Kyösti, J. Meinilä, L. Hentilä, X. Zhao, T. Jämsä, C. Schneider, M. Narandzić, M. Milojević, A. Hong, J. Ylitalo, V.-M. Holappa, M. Alatossava, R. Bultitude, Y. Jong, and T. Rautiainen, "WINNER II channel models," Eur. Commission, Tech. Rep. IST-4-027756, Sep. 2007.
[4] L. Liu, C. Oestges, J. Poutanen, K. Haneda, P. Vainikainen, F. Quitin, F. Tufvesson, and P. D. Doncker, "The COST 2100 MIMO channel model," *IEEE Wireless Commun.*, vol. 19, no. 6, pp. 92–99, Dec. 2012.
[5] T. Rappaport, *Wireless Communications: Principles Practice*, 2nd ed. Upper Saddle River, NJ, USA: Prentice-Hall, 2001.
[6] *Study Channel Model for Frequencies From 0.5 to 100 GHz*, document 3GPP 38.901, V1.0.1, Mar. 2017.
[7] "Measurement results and final mmMAGIC channel models," Eur. Commission, Tech. Rep. H2020-ICT-671650-mmMAGIC/D2.2, May 2017.
[8] V. Nurmela, A. Karttunen, A. Roivainen, L. Raschkowski, V. Hovinen, J. Y. Eb, N. Omaki, K. Kusume, A. Hekkala, and R. Weiler, "Deliverable D1.4 METIS channel models," in *Proc. Mobile Wireless Commun. Enablers Inf. Soc. (METIS)*, Feb. 2015, p. 1.
[9] A. Maltsev, *Channel Models for 60 GHz WLAN Systems*, document 802.11-09/0334r8, May 2010.
[10] A. Maltsev, A. Pudeyev, A. Lomayev, and I. Bolotin, "Channel modeling in the next generation mmWave Wi-Fi: IEEE 802.11ay standard," in *Proc. 22nd Eur. Wireless Conf.*, May 2016, pp. 1–8.
[11] C. Gustafson, K. Haneda, S. Wyne, and F. Tufvesson, "On mm-wave multipath clustering and channel modeling," *IEEE Trans. Antennas Propag.*, vol. 62, no. 3, pp. 1445–1455, Mar. 2014.
[12] A. Maltsev, "Channel modeling and characterization-MiWEBA," Tech. Rep. FP7-ICT-608637, Jun. 2014.
[13] M. K. Samimi and T. S. Rappaport, "3-D millimeter-wave statistical channel model for 5G wireless system design," *IEEE Trans. Microw. Theory Techn.*, vol. 64, no. 7, pp. 2207–2225, Jul. 2016.
[14] D. Dupleich, N. Iqbal, C. Schneider, S. Häfner, R. Müller, S. Skoblikov, J. Luo, and R. S. Thomä, "Investigations on fading scaling with bandwidth and directivity at 60 GHz," in *Proc. 11th Eur. Conf. Antennas Propag. (EUCAP)*, Mar. 2017, pp. 3375–3379.
[15] D. Dupleich, N. Iqbal, C. Schneider, S. Häfner, R. Müller, S. Skoblikov, J. Luo, G. Delgaldo, and R. S. Thomä, "Influence of system aspects on fading at mm-waves," *IET Microw., Antennas Propag.*, vol. 12, no. 4, pp. 516–524, 2018.
[16] N. Iqbal, D. Dupleich, C. Schneider, J. Luo, R. Müller, S. Häfner, G. Del Galdo, and R. S. Thomä, "Modeling of intra-cluster multipaths for 60 GHz fading channels," in *Proc. 12th Eur. Conf. Antennas Propag. (EuCAP)*, Apr. 2018, pp. 1–5.
[17] N. Iqbal, J. Luo, D. Dupleich, S. Häfner, R. Müller, C. Schneider, and R. S. Thomä, "Second-order statistical characterization of the 60 GHz cluster fading channels," in *Proc. IEEE 29th Annu. Int. Symp. Pers., Indoor Mobile Radio Commun. (PIMRC)*, Sep. 2018, pp. 241–245.
[18] R. Müller, R. Herrmann, D. A. Dupleich, C. Schneider, and R. S. Thomä, "Ultrawideband multichannel sounding for mm-wave," in *Proc. 8th Eur. Conf. Antennas Propag. (EuCAP)*, Apr. 2014, pp. 817–821.

[19] M. Zhu, "Geometry-based radio channel characterization and modeling: Parameterization, implementation and validation," Ph.D. dissertation, Dept. Elect. Inf. Technol., Radio Syst.-lup-obsolete (research group), Lund Univ., Lund, Sweden, 2014.
[20] A. F. Molisch, *Wireless Communications*, 2nd ed. Hoboken, NJ, USA: Wiley, 2011.
[21] A. Böttcher, C. Schneider, P. Vary, and R. S. Thomä, "Dependency of the power and delay domain parameters on antenna height and distance in urban macro cell," in *Proc. 5th Eur. Conf. Antennas Propag. (EUCAP)*, Apr. 2011, pp. 1395–1399.
[22] D. A. Dickey and W. A. Fuller, "Distribution of the estimators for autoregressive time series with a unit root," *J. Amer. Statist. Assoc.*, vol. 74, no. 366a, pp. 427–431, 1979.
[23] A. F. Molisch, "Ultra-wide-band propagation channels," *Proc. IEEE*, vol. 97, no. 2, pp. 353–371, Feb. 2009.
[24] M. V. Clark and L. J. Greenstein, "The relationship between fading and bandwidth for multipath channels," *IEEE Trans. Wireless Commun.*, vol. 4, no. 4, pp. 1372–1376, Jul. 2005.
[25] B. Picinbono and P. Bondon, "Second-order statistics of complex signals," *IEEE Trans. Signal Process.*, vol. 45, no. 2, pp. 411–420, Feb. 1997.
[26] P. J. Schreier and L. L. Scharf, "Second-order analysis of improper complex random vectors and processes," *IEEE Trans. Signal Process.*, vol. 51, no. 3, pp. 714–725, Mar. 2003.
[27] L. Franks, "Carrier and bit synchronization in data communication—A tutorial review," *IEEE Trans. Commun.*, vol. COM-28, no. 8, pp. 1107–1121, Aug. 1980.
[28] I. Kochanska, "Testing the wide-sense stationarity of bandpass signals for underwater acoustic communications," in *Proc. IEEE Int. Conf. Innov. Intell. Syst. Appl. (INISTA)*, Jul. 2017, pp. 484–489.
[29] N. Iqbal, C. Schneider, J. Luo, D. Dupleich, R. Müller, S. Häfner, and R. S. Thomä, "On the stochastic and deterministic behavior of mmwave channels," in *Proc. 11th Eur. Conf. Antennas Propag. (EUCAP)*, Mar. 2017, pp. 1813–1817.
[30] N. Iqbal, J. Luo, C. Schneider, D. Dupleich, R. Müller, S. Häfner, and R. S. Thomä, "Stochastic/deterministic behavior of cross polarization discrimination in mmwave channels," in *Proc. IEEE ICC Wireless Commun. Symp. (ICC)*, May 2017, pp. 1–5.
[31] N. Iqbal, J. Luo, R. Müller, G. Steinböck, C. Schneider, D. Dupleich, S. Häfner, and R. S. Thomä, "Multipath cluster fading statistics and modeling in millimeter wave radio channels," *IEEE Trans. Antennas Propag.*, vol. 67, no. 4, pp. 2622–2632, Jan. 2019.
[32] W. Q. Malik, "Polarimetric characterization of ultrawideband propagation channels," *IEEE Trans. Antennas Propag.*, vol. 56, no. 2, pp. 532–539, Feb. 2008.

NAVEED IQBAL (S'17) received B.Sc. degree in electronics from Quaid-e-Azam University, Islamabad, Pakistan, in 2008, and the M.Sc. degree in communications and signals processing from the Technische Universität Ilmenau, Ilmenau, Germany, in 2014. Since 2015, he has been a doctoral candidate with the German Research Center, Huawei Technologies Düsseldorf GmbH, Munich, Germany. He is currently working in the field of channel models for millimeter wave systems. His research interests are in the field of channel measurements and modeling for mmWave communication systems, low complexity deterministic/randomized algorithms for antenna subset selection, and beamforming techniques for MIMO systems. He has been involved in the mmMAGIC project. He has contributed to the development of mmMAGIC, IEEE 802.11ay, and 3GPP TR 37.885 channel models. He has coauthored two Best Research Paper Award-winning papers at the European Wireless Conference, in 2013, and the European Conference of Antennas and Propagation, in 2017.

JIAN LUO received the B.Sc. degree in communications engineering from the South China University of Technology, Guangzhou, China, in 2004, and the M.Sc. and Ph.D. degrees in electrical engineering from Technische Universität Berlin, Berlin, Germany, in 2006 and 2012, respectively. From 2007 to 2012, he was a Researcher with the Fraunhofer Heinrich Hertz Institute, Berlin, Germany, and was involved in several German national and EU funded projects, including EASY-A, SMART-RF, and SAPHYRE. Since 2012, he has been with the German Research Center, Huawei Technologies Düsseldorf GmbH, Munich, Germany, where he has been working on 5G wireless communication systems. He has been involved in EU H2020 5GPPP METIS, mmMAGIC, 5GCAR, and 5G-VINNI projects. In mmMAGIC, he led the air-interface design. His current research interests include channel measurement and modeling, 5G systems, especially millimeter wave, and 5G for V2X/vertical industry.

CHRISTIAN SCHNEIDER received the Diploma degree in electrical engineering from Technische Universität Ilmenau, Ilmenau, Germany, in 2001, where he is currently pursuing the Ph.D. degree with the Institute for Information Technology. His current research interests include wireless multidimensional channel sounding, channel characterization and analysis, channel modeling for single-link and multilink cases in cellular and vehicular networks at microwave and millimeter–wave bands, space-time signal processing, adaptive techniques, and passive coherent localization. He was a recipient of the Best Paper Award at the European Wireless Conference, in 2013, and the European Conference of Antennas and Propagation, in 2017.

DIEGO ANDRES DUPLEICH received the engineering degree in electronic engineering from the Universidad Tecnológica Nacional, Paraná, Argentina, in 2009, and the M.Sc. degree (Hons.) in communications and signal processing from Technische Universität Ilmenau, Ilmenau, Germany, in 2013, where he is currently pursuing the Ph.D. degree in electrical engineering. From 2009 to 2010, he was an RF Specialist in satellite communications with the Emerging Markets Communications, Raisting, Germany. Since 2013, he has been with the Electronic Measurement Research Laboratory, Technische Universität Ilmenau, where he is currently involved in the millimeter-wave field.

ROBERT MÜLLER received the M.S. degree in electronic engineering from the Berlin University of Technology, Berlin, Germany, in 2009. His areas of interests include high-frequency components design. Furthermore, he is also involved in high-frequency front-end design, antenna design, ultrawide-band system design, and special antenna array design for channel sounding applications. His current research interests include channel sounding measurements systems and analysis for further communication systems in the field of V2V and cellular networks.

STEPHAN HÄFNER received the M.Sc. degree in computer engineering from Technische Universität Ilmenau, Ilmenau, Germany, in 2012, where he is currently pursuing the Ph.D. degree. Since 2012, he has been with the Electronic Measurement Research Laboratory, Technische Universität Ilmenau. His current research interests include array signal processing, and high-resolution parameter estimation for channel sounding and radar applications.

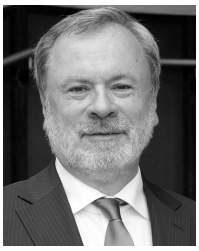

REINER S. THOMÄ (M'92–SM'99–F'07) received the Dipl.Ing. (M.S.E.E.), Dr. Ing. (Ph.D.E.E.), and Dr. Ing. habil. degrees in electrical engineering and information technology from Technische Hochschule Ilmenau, Ilmenau, Germany, in 1975, 1983, and 1989, respectively. From 1975 to 1988, he was a Research Associate in the fields of electronic circuits, measurement engineering, and digital signal processing with Technische Hochschule Ilmenau. From 1988 to 1990, he was a Research Engineer with the Akademie der Wissenschaften der DDR (Zentrum für Wissenschaftlichen Gerätebau), Berlin, Germany, where he was involved in radio surveillance. In 1991, he spent a sabbatical leave at the University of Erlangen–Nürnberg (Lehrstuhl für Nachrichtentechnik), Erlangen, Germany. Since 1992, he has been a Professor of electrical engineering (electronic measurement) with TU Ilmenau, where he was the Director of the Institute of Communications and Measurement Engineering, from 1999 to 2005. With his group, he has contributed to several European and German research projects and clusters such as RESCUE, WINNER, PULSERS, EUWB, NEWCOM, COST 273, 2100, IC 1004, COSR IRACON, EASY-A, and EASY-C. He was the Speaker of the German nationwide DFG-focus project UKoLOS, Ultra-Wideband Radio Technologies for Communications, Localization, and Sensor Applications (SPP 1202). His current research interests include measurement and digital signal processing methods (correlation and spectral analysis, system identification, sensor arrays, compressive sensing, and time-frequency, and cyclostationary signal analysis), their application in mobile radio and radar systems (multidimensional channel sounding, propagation measurement and parameter estimation, MIMO-, mm-wave-, and ultrawideband radar), measurement-based performance evaluation of MIMO transmission systems, including over-the-air testing in virtual electromagnetic environments, passive coherent location, and UWB radar sensor systems for object detection, tracking, and imaging. He is a member of the URSI (Comm. A), VDE/ITG. He was an Advisory Board Member of EU project mmMAGIC. Since 1999, he has been the Chair of the IEEE-IM TC-13 on Measurement in Wireless and Telecommunications. He was a recipient of the Thuringian State Research Award for Applied Research both for contributions to high-resolution multidimensional channel sounding, in 2007, and the Vodafone Innovation Award, in 2014.